Inorganic Chemistry

Article

pubs.acs.org/IC

High-Resolution Solid-State Oxygen-17 NMR of Actinide-Bearing Compounds: An Insight into the 5f Chemistry

Laura Martel,*[,†] Nicola Magnani,[†] Jean-Francois Vigier,[†] Jacobus Boshoven,[†] Chris Selfslag,[†] Ian Farnan,[‡] Jean-Christophe Griveau,[†] Joseph Somers,[†] and Thomas Fanghänel[†]

[†]European Commission, Joint Research Centre, Institute for Transuranium Elements, Hermann-von-Helmoltz-Platz 1, D-76344 Eggenstein-Leopoldshafen, Germany

[‡]Department of Earth Sciences, University of Cambridge, Downing Street, Cambridge, CB2 3EQ, U.K.

Supporting Information

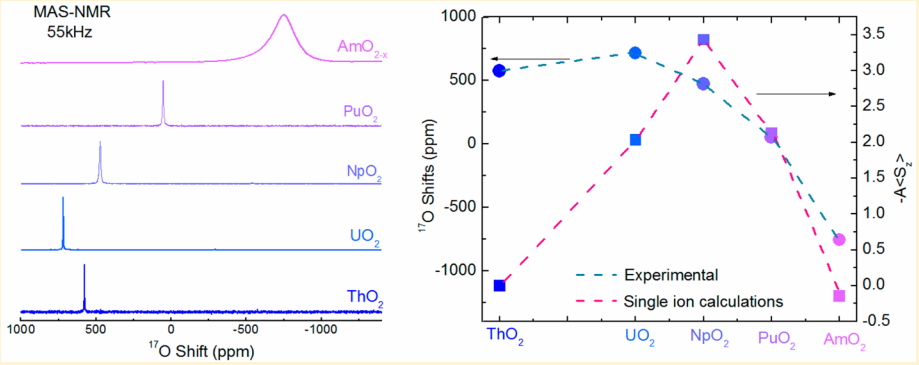

ABSTRACT: A massive interest has been generated lately by the improvement of solid-state magic-angle spinning (MAS) NMR methods for the study of a broad range of paramagnetic organic and inorganic materials. The open-shell cations at the origin of this paramagnetism can be metals, transition metals, or rare-earth elements. Actinide-bearing compounds and their 5f unpaired electrons remain elusive in this intensive research area due to their well-known high radiotoxicity. A dedicated effort enabling the handling of these highly radioactive materials now allows their analysis using high-resolution MAS NMR (>55 kHz). Here, the study of the local structure of a series of actinide dioxides, namely, ThO_2, UO_2, NpO_2, PuO_2, and AmO_2, using solid-state ^{17}O MAS NMR is reported. An important increase of the spectral resolution is found due to the removal of the dipolar broadening proving the efficiency of this technique for structural analysis. The NMR parameters in these systems with numerous and unpaired 5f electrons were interpreted using an empirical approach. Single-ion model calculations were performed for the first time to determine the *z* component of electron spin on each of the actinide atoms, which is proportional to the shifts. A similar variation thereof was observed only for the heavier actinides of this study.

INTRODUCTION

With about 13% of electrical power generated worldwide from nuclear reactors,[1] qualified performance and safety of nuclear fuels require a detailed knowledge of actinide oxide chemistry, which must be backed by high-resolution element-specific spectroscopies and reinforced by theory.[1−3] An atomic-scale analysis of nuclear fuels (UO_2 and mixed oxide (MOX)) and irradiated fuels is a key to these improvements.[1,4−6] The understanding of nuclear fuel in terms of structural chemistry and radiation damage has relied in the past on classical techniques such as X-ray diffraction (XRD), which only provide part of the understanding needed to fully comprehend the fuel behavior. Probing the atomic scale with techniques such as X-ray absorption spectroscopy and now magic-angle spinning (MAS) NMR allows us even greater insight into these materials. So far, most of the solid-state NMR studies on transuranic compounds have been performed under static conditions,[7−10] with their lack of resolution for structural analysis. MAS NMR is nowadays a method of choice for atomic-scale studies,[11] but its use for highly radioactive materials has been hampered by safety issues related to their handling and the contamination risks in the case of a high-speed rotor crash. The promise of the MAS NMR method has been demonstrated using a cumbersome triple-containment rotor system.[12,13] A major breakthrough has now been achieved, and one MAS NMR spectrometer in the world has been developed for these applications on a routine basis;[14] it can use state-of-the-art probes operating at the technological cutting edge enabling the highest spectral resolution.[15]

In paramagnetic compounds, a rigorous interpretation of the NMR spectra for open-shell cations as metals,[16] transition metals (3d),[17] or rare earth (4f)[18−20] is enabled by combining solid-state MAS NMR[21,22] with state-of-the-art density func-

Received: April 2, 2014
Published: June 13, 2014

   dx.doi.org/10.1021/ic5007555 | Inorg. Chem. 2014, 53, 6928−6933

tional theory (DFT) calculations.[23−26] Though DFT calculations of actinide-bearing molecules has been used occasionally for the interpretation of liquid-state NMR,[27,28] there are only two papers on such studies for solid-state NMR, and both are limited to closed 5f-shell materials.[29,30] This absence of such theoretical studies is due to various difficulties,[31] specifically, number of electrons to deal with, introduction of spin−orbit coupling, a large number of near-degenerate states close in energy to the ground state,[32,33] and the obvious lack of experimental data making solid-state NMR calculations not yet possible in 5f open-shell systems. Recent work by Wall et al.[34] and Autillo et al.[35] show that it is possible to understand the paramagnetic shifts in liquid-state NMR of actinide compounds. Nevertheless, the Evans method[36] used in these studies cannot be extended to a high-resolution solid-state NMR study, mainly due to technical difficulties (i.e., presence of a liquid internal and external reference to the sample, significant variation of the probe temperature (from 278 to 323 K[34]) during spinning, and incorporation into a radioactive glovebox).

Herein, we report the elucidation of the ^{17}O NMR parameters (i.e., longitudinal relaxation time T_1, line broadening, and shifts) on a series of actinide dioxides, namely, ThO_2 ($5f^0$), UO_2 ($5f^2$), NpO_2 ($5f^3$), PuO_2 ($5f^4$), and AmO_2 ($5f^5$), enriched in oxygen-17 using empirical equations. We demonstrate the capability to acquire MAS NMR spectra at very high spinning frequencies (up to 55 kHz), with concomitant highest resolution, on such highly radioactive compounds (activity of 9.35×10^8 Bq for AmO_2). The results of the single-ion model calculations calculated for the first time for $\langle S_z \rangle$ exhibit a similar trend with the shifts for the heavy actinide dioxides but not for "closed shell" ThO_2.

EXPERIMENTAL SECTION

All the samples, except for the UO_2, were sintered at 1650 °C during 4 h under Ar/H_2 to ensure a high crystallinity. As the oxygen-17 isotope has a natural abundance of 0.037%, all the samples were enriched using the gas exchange technique,[37] which involved thermal treatment at 800 °C during 24 h under an $^{17}O_2/Ar$ atmosphere. In the case of NpO_2, it has been shown that during the cooling, the sample can be oxidized; therefore, the cooling was performed under Ar. For UO_2, to avoid higher oxidation states, the sample was enriched in ^{17}O by the same method and then sintered in Ar/H_2 to yield the stoichiometric material.

The purity of all of the samples was checked by powder XRD using a dedicated Bruker D8 Advance diffractometer (Cu Kα radiation, 40 kV, and 40 mA), implanted in a radioactive glovebox, with a Bragg−Brentano $\theta/2\theta$ configuration and equipped with a curved Ge monochromator (1, 1, 1) and a Lynxeye linear position-sensitive detector. The powder patterns were recorded using a step size of 0.0197° across the angular range of $10° \leq 2\theta \leq 120°$ on about 15 to 20 mg of a prepared powder sample. For NpO_2, PuO_2, and AmO_{2-x} the powders were loaded in an epoxy resin to fix them and prevent their dispersion. For ThO_2, UO_2, NpO_2, and PuO_2 only one cubic fluorite ($Fm\bar{3}m$) phase was identified with lattice parameters of 5.5975, 5.4704, 5.4340, and 5.3977 Å, respectively. All are very similar to that found in the literature.[38−41] The case of the AmO_{2-x} sample will be discussed in the main text.

The ^{17}O NMR experiments were performed on a 9.4 T Bruker spectrometer at the Larmor frequency of 54.25 MHz. The standard 1.3 mm Bruker MAS NMR probe is located in a radioactive glovebox, as described in ref 14, allowing the acquisition of high-resolution spectra of these highly radioactive materials. All the spectra were acquired using a synchronized Hahn-echo pulse sequence. The pulse durations were 4 μs ($\pi/2$) and 8 μs (π), with an echo delay of 18.2 μs (1 rotor period). All spectra were calibrated relative to water H_2O enriched in ^{17}O (0 ppm). The relaxation time was determined using an inversion−recovery pulse sequence. All the spectra were analyzed and fitted using the dmfit software.[42]

RESULTS AND DISCUSSIONS

The ^{17}O static and 55 kHz MAS NMR spectra of the actinide dioxide series (^{232}Th, ^{238}U, ^{237}Np, ^{239}Pu, ^{241}Am) are presented in Figure 1. Because of their cubic fluorite structure, the

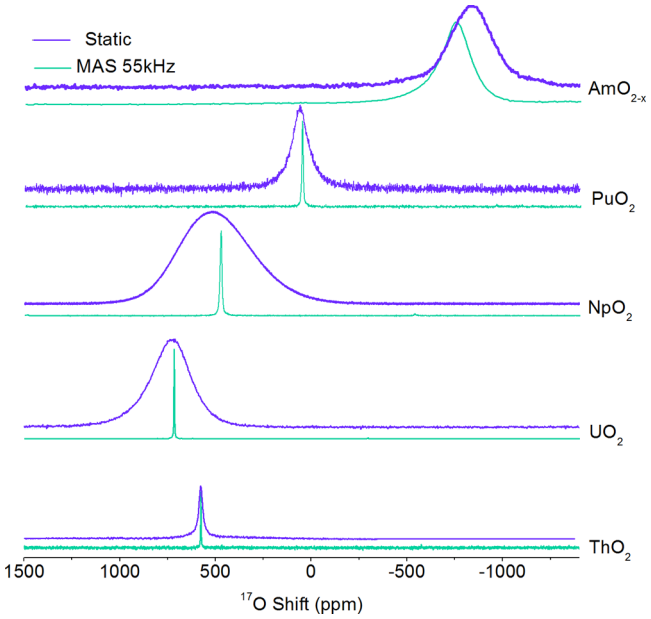

Figure 1. ^{17}O static (purple) and 55 kHz (green) MAS NMR spectra of the five actinide dioxides.

quadrupolar coupling constant is zero (i.e., there is no second-order quadrupolar line shape), and a single feature is expected. The MAS NMR spectrum of ThO_2 was acquired for the first time, and its signal presents a sharp line (3 ppm) at 576 ppm. This shift is in the typical range expected for metal dioxides with four-coordinated oxygen (Supporting Information, Figure S1). A single feature was also detected at 717, 475, and 54 ppm in the MAS NMR spectra of UO_2, NpO_2, and PuO_2, respectively (Table 1). The XRD pattern and the MAS NMR

Table 1. ^{17}O NMR Shifts of the Five Actinide Dioxides

compound	shifts (ppm)
ThO_2	576
UO_2	717
NpO_2	475
PuO_2	54
AmO_2	−754

spectrum for the AmO_{2-x} sample are shown in Figure 2. Two fluorite phases with lattice parameters of 5.3785(1) and 5.3888(2) Å were identified (Figure 2a) and are a consequence of the sample preparation procedure. According to Lebreton et al.[43] the first phase can be attributed to $AmO_{2.00}$, and the second one can be attributed to hypostoichiometric AmO_{2-x}. A Rietveld refinement indicates that their relative concentrations are 76% (P1—the AmO_2 phase) and 24% (P2—substoichiometric phase) given an uncertainty of 5%. The ^{17}O MAS NMR spectrum was fitted using Gaussian line shapes and the main line, and the spinning sidebands, corresponding to the satellite transitions, were fitted using the "spinning sidebands" option in

dx.doi.org/10.1021/ic5007555 | Inorg. Chem. 2014, 53, 6928−6933

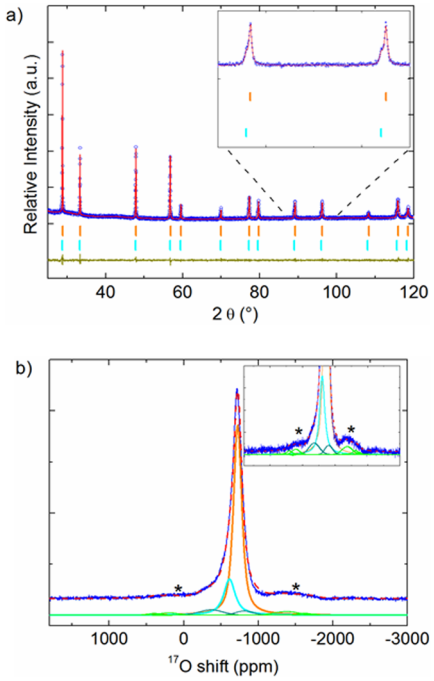

Figure 2. (a) XRD pattern of americium dioxide sample (blue circle) with the corresponding Rietveld refinement. The difference between the experimental and calculated intensities, and the Bragg reflections are marked in orange for $AmO_{2.00}$ and in cyan for AmO_{2-x} phases. (b) ^{17}O MAS NMR spectrum of AmO_{2-x} (blue) and its fit (dashed red line); the peaks are attributed to ordered $AmO_{2.00}$ (orange) and AmO_{2-x} (cyan) phases; additional peaks are due to disorder (dark cyan); spinning sidebands are due to satellite transitions (stars). A zoom on this spectral region is shown in inset.

dmfit. Examination of this spectrum (Figure 2b) reveals a 68% concentration for the peak at −754 ppm enabling it to be attributed to the stoichiometric phase (P1 in XRD). Three additional peaks at −613, −364, and −812 ppm are identified. The fitting procedure, including peak shape and contributions from spinning side bands, identifies the feature at −613 ppm as the contribution of the substoichiometric P2 phase (21% of the total signal). The remaining two peaks (in total 10% of the signal) are attributed to oxygen in disordered phases, possibly caused by self-irradiation damage. In the following discussion, we consider the main peak (P1 phase) only and designate it "AmO_2." The static and MAS shifts in the AmO_2 spectra differ by about 100 ppm, which is attributed to the sensitivity of the paramagnetic shift to the sample temperature (ca. 313 K), which increases with spinning speed (see correlation in Supporting Information, Figure S2). Similar temperature-driven effects have been observed in static investigations performed at low temperatures.[44]

The variation of the longitudinal relaxation time (T_1) at 55 kHz with the increasing number of 5f electrons in the actinide dioxides is presented in Figure 3. ThO_2 has a long T_1 (1015 s), an attribute of its diamagnetic character. The remaining samples possess a much shorter T_1 (<1s), a characteristic of paramagnetic samples.[45] For PuO_2, only one paper refers to its magnetic susceptibility,[46] showing, surprisingly, that it is constant and positive in all temperature ranges (i.e., Van Vleck paramagnetism). This fundamental difference to paramagnetic UO_2, NpO_2, and AmO_2 and diamagnetic ThO_2 is also revealed in the relaxation time measurements presented here.

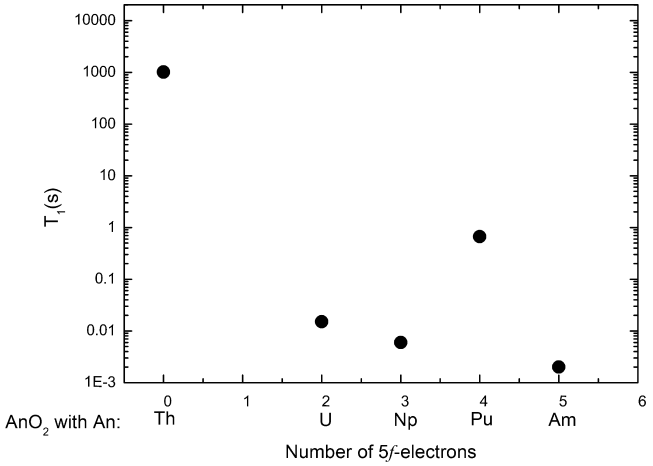

Figure 3. Variation of the longitudinal relaxation time, T_1, with 5f-electron occupation in the actinide dioxides.

The variation of the full width at half-maximum (fwhm) of the five actinide dioxides is presented in Figure 4. A clear

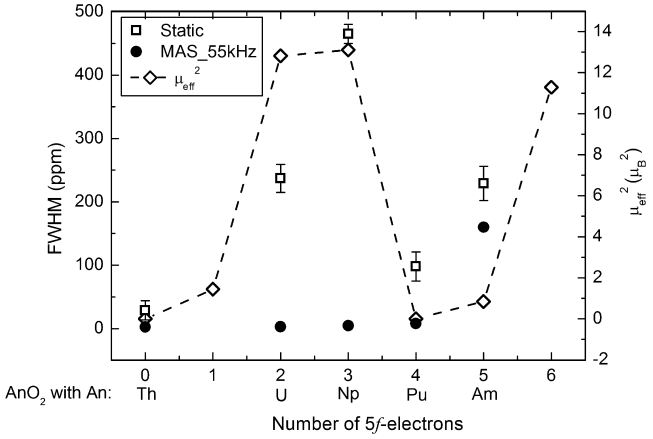

Figure 4. Variation of the full width at half-maximum (fwhm) and of the square of the effective magnetic moment (μ_{eff}^2) as a function of f-electron occupation. The dashed line is a guide for the eye linking all of the μ_{eff}^2 data points.

improvement of the spectral resolution (i.e., decrease of the line width) is observed at a MAS rate of 55 kHz. The remaining line broadening in AmO_2 is likely linked to the presence of two phases and to a local disorder in the sample due to its nonstoichiometry, that is, distribution of vacancies in the AmO_{2-x} phase. Similar effects have been observed in NMR data of other paramagnetic compounds.[47] If the anisotropic shift due to the electron−nuclear dipolar interaction is the dominant term in determining the line width, then the fwhm of the static NMR signal and the square of the effective magnetic moment (μ_{eff}^2) should exhibit a similar behavior. This interaction has an angular dependence, and for a nucleus at a distance r from the paramagnetic ion, it is given by[48]

$$H_d = \alpha(3\cos^2\theta - 1)/r^3 \quad (1)$$

with $\alpha = \mu_{eff}^2 H_0/3kT$, where θ is the angle between the magnetic field (H_0) and the axis linking the paramagnetic ion and the nucleus, k is the Boltzmann constant, and T is the temperature. Indeed, the fwhm and μ_{eff}^2 values, obtained from refs 49 and 63, exhibit a similar dependence on the f-electron

dx.doi.org/10.1021/ic5007555 | Inorg. Chem. 2014, 53, 6928−6933

occupation (see Figure 4), confirming the domination of the dipolar interaction in the broadening. As ThO_2 is diamagnetic (i.e., $\mu = 0$), the fwhm is very small. The maximum of μ_{eff}^2 is found for NpO_2 ($5f^3$), while the fwhm and μ_{eff} decrease for PuO_2, with its nonmagnetic ground state, and increase again for AmO_{2-x}.

The paramagnetic shift is dependent on the bond angle and/or the cation−anion distances.[25] As these dioxide compounds possess a fluorite structure, the only variable is the actinide−oxide distance (d_{An-O}), which is plotted against the shifts in Supporting Information, Figure S3. The paramagnetic shift tends to decrease with decreasing An−O distance, that is, along the actinide series; this representation will be essential for the interpretation of the NMR data of actinide dioxide solid solutions (cf. similar studies on the rare-earth-bearing compounds[50]). The shifts measured here were compared with those reported in static conditions by Tokunaga et al.[44,51−53] and Eastman et al.[54] For UO_2, NpO_2, and PuO_2, the results are quite similar. For AmO_2, the difference in shift is probably caused by the differences in the samples themselves (e.g., stoichiometry and irradiation-induced damage[44]) and also by the heating induced by the sample rotation.

Because of the pure cubic symmetry, only the through-bond (Fermi-contact) interaction between the paramagnetic actinide nuclei and the ^{17}O nuclei determines the shift.[54] In the lanthanides, this Fermi-contact interaction is characterized by a single reversal of the sign of the shift across the 4f series.[19,55] The change of the ^{17}O shifts in lanthanide sesquioxides (Ln_2O_3) and actinide dioxides (AnO_2) as a function of the number of f electrons is presented in Supporting Information, Figure S4. In contrast to the lanthanides, where the sign change occurs at gadolinium ($5f^7$),[56,55] in the actinides, this phenomenon occurs already at americium ($5f^5$) for the actinide dioxides, most likely indicating that f-electron delocalization plays an important role. This behavior of the shift in the Ln_2O_3 series has been explained by Golding and Halton, who calculated the thermal average of the z-component of electron spin on each Ln atom, $\langle S_z \rangle$, and found that its variation follows the shift behavior.[56] This parameter, $\langle S_z \rangle$, is linked to the effective magnetic field ΔH at the NMR nucleus with the unpaired 5f electrons by[54,55,57]

$$\Delta H = A_s \langle S_z \rangle / \gamma h \quad (2)$$

where A_s is the electron−nucleus transferred hyperfine coupling constant, γ is the gyromagnetic ratio of the observed nucleus, and h is the Planck constant.

In the absence of any other approach to understand these shifts, we followed the method of Golding and Halton, and we calculated $\langle S_z \rangle$ for the first time for each member of the actinide dioxide family using a single-ion model.[58] The full Hamiltonian representing the $5f^n$ configuration of each tetravalent actinide ion (n = 2,...,5 for An = U,...,Am) can be written as[59]

$$H = H_{FI} + H_{CF} + H_Z \quad (3)$$

where H_{FI} includes the combined effect of the actinide free-ion terms (such as the Coulomb repulsion and the spin−orbit interaction). The Hamiltonian of the cubic crystal-field potential due to the oxygen ligands (values of B_4 and B_6 given in Supporting Information, Table S1) has the form[58]

$$H_{CF} = B_4 \lfloor C_0^{(4)} + \sqrt{5/14}\,(C_4^{(4)} + C_{-4}^{(4)}) \rfloor + B_6 \lfloor C_0^{(6)} - \sqrt{7/2}\,(C_4^{(6)} + C_{-4}^{(6)}) \rfloor \quad (4)$$

Finally, the Zeeman term associated with the applied magnetic field H_0 is described by the following Hamiltonian:

$$H_Z = -\mu_B H_0 (L_Z + 2S_Z) \quad (5)$$

The entire Hamiltonian was diagonalized numerically, so that intermediate coupling and J-mixing effects are taken into account naturally in the calculations (see Supporting Information, Table S1). The free-ion and crystal-field parameters were fixed to those determined by inelastic neutron scattering for UO_2, NpO_2, and PuO_2[60−62] and by magnetic susceptibility measurements for AmO_2.[63] As covalency effects are not required to interpret such data, we have not included them in our calculations. Nevertheless, we did check that adding a reasonable orbital reduction factor does not qualitatively change our results. The thermal average $\langle S_z \rangle$ was calculated at 340 K, based on the estimates of the sample heating due to spinning (see Supporting Information, Figure S2). Although the precise experimental temperature is undetermined, we checked that the calculated values of $k_B T \langle S_z \rangle$ do not vary much (3% for PuO_2 and less than 1% for the other dioxides within a range of ±10 K). Similarly, H_0 was fixed at the experimental value of 9.4 T, but the calculated values of $\langle S_z \rangle / H_0$ had no significant effect as expected.

We assumed, like Golding and Halton did for the lanthanides, that the hyperfine coupling constant (A_s) was constant through the actinide series. Some previous work on UO_2[9] and NpO_2[53] shows that this parameter is negligible, and as it is not known for PuO_2 and AmO_2 it was also considered as very small. The change of $-3k_B T \langle S_z \rangle / \mu_B H_0$ and of the ^{17}O paramagnetic shifts is plotted against the $5f^n$ electron occupation in Figure 5. A very similar trend between the calculated and measured values holds for the heavier actinide dioxides of Np, Pu, and Am. For UO_2 the value is qualitatively in line with the predictions. The trend does not hold for ThO_2, however, indicating that the nonmagnetic ground state of ThO_2 is more complicated than a simple "empty f shell."[64−67] Furthermore, $\langle S_z \rangle$ does not change sign at AmO_2 ($5f^5$) implying that the 5f electrons are indeed more complicated to handle theoretically than the 4f electrons in the lanthanide series.

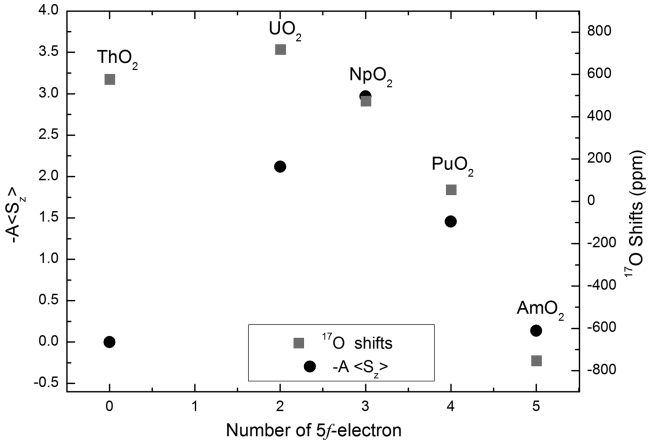

Figure 5. Plot of $-A \langle S_z \rangle$ and the ^{17}O shifts against 5f-electron occupation. A is a constant equal to $-3kT/\mu_B H_0$.

dx.doi.org/10.1021/ic5007555 | Inorg. Chem. 2014, 53, 6928−6933

CONCLUSION

This work demonstrated the first acquisition of high-resolution MAS NMR spectra for a series of highly radioactive materials. The ^{17}O spectra of ThO_2 acquired for the first time exhibits a sharp line consistent with its diamagnetic behavior and a shift at 576 ppm. For the AmO_{2-x} sample, we observe a strong sensitivity of the shift to composition, temperature, and of course radiation damage in the form of disorder, which is a particular capability of MAS NMR we are actively pursuing. The expected sign change in the shifts through the series due to the Fermi-contact interaction already occurs at americium ($5f^5$) for the actinide dioxides, while for the lanthanides its occurs at gadolinium ($5f^7$). On the basis of empirical equations, we provided an understanding of this variation of the shifts through the actinide dioxide series. Thus, the shifts correlate with $\langle S_z \rangle$, which was calculated for the first time for each actinide dioxide. While the heavier actinide dioxides exhibit a similar trend between the shift and $\langle S_z \rangle$, ThO_2 does not, indicating that it exhibits a more complicated behavior than that of an empty f shell.

This work clearly demonstrates the importance and potential of MAS NMR for the understanding of atomic-scale features in highly radioactive materials and opens new possibilities to assess fresh and irradiated fuels, nuclear waste forms, and radioactive contaminated environmental samples. Our next goals focus on local structure in actinide dioxide solid solutions and in dedicated irradiation damage studies to reveal the intricacies of such materials when exposed to extreme conditions. This study definitely extends the field of paramagnetic NMR to 5f-electron compounds, which possess different chemical and physical properties than the other paramagnetic compounds. Finally, these experiments and their modeling can also be used in liquid-state NMR, for which numerous actinide compounds are under study;[28,68] as noticed here, some discrepancies with lanthanides have been observed too.[69,34] Indeed, these calculations and experimental data are essential for the development of NMR DFT calculations for the complex 5f electron systems.

Caution! *As all these actinide dioxides, especially the ^{237}Np, ^{239}Pu, and ^{241}Am, present considerable radiotoxicity hazards, they were all handled under carefully controlled dedicated laboratories at the Institute for Transuranium Elements in Karlsruhe. All steps were performed in hermetically sealed gloveboxes maintained at an under pressure with respect to the laboratory.*

ASSOCIATED CONTENT

Supporting Information

Illustrations of data to indicate comparison of oxygen-17 shifts, temperature change with spinning speed, oxygen-17 shifts as a function of An−O distance, changes in oxygen-17 shifts as a function of the number of f electrons. Table of crystal field data associated with Th, U, Np, Pu, and Am oxides. Additional references. This material is available free of charge via the Internet at http://pubs.acs.org.

AUTHOR INFORMATION

Corresponding Author

*E-mail: laura.martel@ec.europa.eu.

Notes

The authors declare no competing financial interest.

ACKNOWLEDGMENTS

We are thankful to D. Bouexière for the help with XRD and to R. Caciuffo, T. Charpentier, R. Eloirdi, and O. Pauvert for fruitful discussions and comments on the manuscript.

REFERENCES

(1) *Nuclear Power Today;* 2012. http://www.world-nuclear.org/info/inf01.html.
(2) Vogel, S. C. *ISRN Mater. Sci.* **2013**, DOI: 10.1155/2013/302408.
(3) Prodan, I. D.; Scuseria, G. E.; Martin, R. L. *Phys. Rev. B* **2007**, *76*, 033101.
(4) Morss, L. R.; Edelstein, N. M.; Fuger, J. *The Chemistry of the Actinides and Transactinides Elements;* 3rd. ed.; Springer: New York, 2006; p 256.
(5) Martin, P.; Grandjean, S.; Valot, C.; Carlot, G.; Ripert, M.; Blanc, P.; Hennig, C. *J. Alloys Compd.* **2007**, *444*−*445*, 410−414.
(6) Belin, R. C.; Martin, P. M.; Lechelle, J.; Reynaud, M.; Scheinost, A. C. *Inorg. Chem.* **2013**, *52*, 2966−2972.
(7) Yasuoka, H.; Koutroulakis, G.; Chudo, H.; Richmond, S.; Veirs, D. K.; Smith, A. I.; Bauer, E. D.; Thompson, J. D.; Jarvinen, G. D.; Clark, D. L. *Science* **2012**, *336*, 901−903.
(8) Curro, N. J.; Caldwell, T.; Bauer, E. D.; Morales, L. A.; Graf, M. J.; Bang, Y.; Balatsky, A. V.; Thompson, J. D.; Sarrao, J. L. *Nature* **2005**, *434*, 622−625.
(9) Ikushima, K.; Tsutsui, S.; Haga, Y.; Yasuoka, H.; Walstedt, R. E.; Masaki, N. M.; Nakamura, A.; Nasu, S.; Onuki, Y. *Phys. Rev. B* **2001**, *63*, 104404.
(10) Walstedt, R. E.; Tokunaga, Y.; Kato, H.; Sakai, H.; Fujimoto, T.; Kambe, S.; Yasuoka, H. *J. Phys. Soc. Jpn.* **2006**, *75*, 77−81.
(11) Emsley, L.; Bertini, I. *Acc. Chem. Res.* **2013**, *46*, 1912−1913.
(12) Farnan, I.; Cho, H.; Weber, W. J. *Nature* **2007**, *445*, 190−193.
(13) Farnan, I.; Cho, H.; Weber, W. J.; Scheele, R. D.; Johnson, N. R.; Kozelisky, A. E. *Rev. Sci. Instrum.* **2004**, *75*, 5232−5236.
(14) Martel, L.; Somers, J.; Berkmann, C.; Koepp, F.; Rothermel, A.; Pauvert, O.; Selfslag, C.; Farnan, I. *Rev. Sci. Instrum.* **2013**, *84*, 055112.
(15) Carvajal Nunez, U.; Martel, L.; Prieur, D.; Lopez Honorato, E.; Eloirdi, R.; Farnan, I.; Vitova, T.; Somers, J. *Inorg. Chem.* **2013**, *52*, 11669−11676.
(16) Knight, M. J.; Felli, I. C.; Pierattelli, R.; Bertini, I.; Emsley, L.; Herrmann, T.; Pintacuda, G. *J. Am. Chem. Soc.* **2012**, *134*, 14730−14733.
(17) Blanc, F.; Leskes, M.; Grey, C. P. *Acc. Chem. Res.* **2013**, *46*, 1952−1963.
(18) Bose, M.; Ganguli, S.; Bhattacharya, M. *Phys. Rev. B* **1979**, *19*, 5535−5548.
(19) Bose, M.; Bhattacharya, M.; Ganguli, S. *Phys. Rev. B* **1979**, *19*, 72−80.
(20) Palke, A. C.; Stebbins, J. F.; Boatner, L. A. *Inorg. Chem.* **2013**, *52*, 12605−12615.
(21) Grey, C. P.; Dupré, N. *Chem. Rev.* **2004**, *104*, 4493−4512.
(22) Knight, M. J.; Felli, I. C.; Pierattelli, R. A.; Emsley, L.; Pintacuda, G. *Acc. Chem. Res.* **2013**, *46*, 2108−2116.
(23) Carlier, D.; Ménétrier, M.; Grey, C. P.; Delmas, C.; Ceder, G. *Phys. Rev. B* **2003**, *67*, 174103.
(24) Castets, A.; Carlier, D.; Zhang, Y.; Boucher, F.; Ménétrier, M. *J. Phys. Chem. C* **2012**, *116*, 18002−18014.
(25) Middlemiss, D. S.; Ilott, A. J.; Clément, R. J.; Strobridge, F. C.; Grey, C. P. *Chem. Mater.* **2013**, *25*, 1723−1734.
(26) Bonhomme, C.; Gervais, C.; Babonneau, F.; Coelho, C.; Pourpoint, F.; Azaïs, T.; Ashbrook, S. E.; Griffin, J. M.; Yates, J. R.; Mauri, F.; Pickard, C. J. *Chem. Rev.* **2012**, *112*, 5733−5779.
(27) Kaupp, M.; Buhl, M.; Malkin, V. G. *Calculation of NMR and EPR Parameters: Theory and Applications;* Wiley: Hoboken, NJ, 2004.
(28) Hrobárik, P.; Hrobáriková, V.; Greif, A. H.; Kaupp, M. *Angew. Chem., Int. Ed.* **2012**, *51*, 10884−10888.
(29) Cho, H.; De Jong, W. A.; Soderquist, C. Z. *J. Chem. Phys.* **2010**, *132*, 084501.

(30) Smith, A. L.; Raison, P. E.; Martel, L.; Charpentier, T.; Farnan, I.; Prieur, D.; Hennig, C.; Scheinost, A.; Konings, R. J. M.; Cheetham, A. K. *Inorg. Chem.* **2014**, *53*, 375−382.
(31) Charpentier, T. *Solid State Nucl. Magn. Reson.* **2011**, *40*, 1−20.
(32) Pyykkö, P. *Chem. Rev.* **1988**, *88*, 563−594.
(33) Schreckenbach, G. P.; Hay, J.; Martin, R. L. *J. Comput. Chem.* **1999**, *20*, 70−90.
(34) Wall, T. F.; Jan, S.; Autillo, M.; Nash, K. L.; Guerin, L.; Le Naour, C.; Moisy, P.; Berthon, C. *Inorg. Chem.*, **2014**, *Article ASAP;* DOI: 10.1021/ic402371x.
(35) Autillo, M.; Kaden, P.; Geist, A.; Guerin, L.; Moisy, P.; Berthon, C.; *Phys. Chem. Chem. Phys.*, **2014**, *Advance Article;* DOI: 10.1039/C4CP00724G.
(36) Evans, D. F. *J. Chem. Soc.* **1959**, 2003−2005.
(37) Ashbrook, S. E.; Smith, M. E. *Chem. Soc. Rev.* **2006**, *35*, 718−735.
(38) Ternary and Polynary Oxides, Thorium, System No. 44. In *Gmelin Handbook of Inorganic Chemistry,* 8th ed.; Springer-Verlag: Berlin, Germany, 1998; Vol. *C2*.
(39) Barrett, S. A.; Jacobson, A. J.; Tofield, B. C.; Fender, B. E. F. *Acta Crystallogr., Sect. B* **1982**, *38*, 2775−2781.
(40) Fahey, J. A.; Turcotte, R. P.; Chikalla, T. D. *Inorg. Nucl. Chem. Lett.* **1974**, *10*, 459−65.
(41) Haschke, J. M.; Allen, T. H.; Morales, L. A. *Science* **2000**, *287*, 285−286.
(42) Massiot, D.; Fayon, F.; Capron, M.; King, I.; Le Calvé, S.; Alonso, B.; Durand, J.-O.; Bujoli, B.; Gan, Z.; Hoatson, G. *Magn. Reson. Chem.* **2002**, *40*, 70−76.
(43) Lebreton, F.; Belin, R. C.; Delahaye, T.; Blanchart, P. *J. Solid State Chem.* **2012**, 196217−224.
(44) Tokunaga, Y.; Nishi, T.; Kambe, S.; Nakada, M.; Itoh, A.; Homma, Y.; Sakai, H.; Chudo, H. *J. Phys. Soc. Jpn.* **2010**, *79*, 053705.
(45) Slichter, C. P. *Principles of Magnetic Resonance,* 2nd ed.; Springer-Verlag: New York, 1980.
(46) Raphael, G.; Lallement, R. *Solid State Commun.* **1968**, *6*, 383−385.
(47) Kim, N.; Stebbins, J. F. *Chem. Mater.* **2007**, *19*, 5742−5747.
(48) Sobel, A. *J. Phys. Chem. Solids* **1967**, *28*, 185−196.
(49) Fournier, J.-M.; Troc, R. *Handbook on the Physics and Chemistry of the Actinides;* Freeman, A. J., Lander, G. H., Eds.; North-Holland: New York, 1985; Vol. *2*.
(50) Grey, C. P.; Smith, M. E.; Cheetham, A. K.; Dobson, C. M.; Dupree, R. *J. Am. Chem. Soc.* **1990**, *112*, 4670−4675.
(51) Tokunaga, Y.; Sakai, H.; Fujimoto, T.; Kambe, S.; Walstedt, R. E.; Ikushima, K.; Yasuoka, H.; Aoki, D.; Homma, Y.; Haga, Y.; Matsuda, T. D.; Ikeda, S.; Yamamoto, E.; Nakamura, A.; Shiokawa, Y.; Nakajima, K.; Arai, Y.; Onuki, Y. *J. Alloys Compd.* **2007**, *444*−*445*, 241−245.
(52) Tokunaga, Y.; Nishi, T.; Kambe, S.; Nakada, M.; Homma, Y.; Sakai, H.; Chudo, H. *Proc. Int. Conf. Heavy Electrons, J. Phys. Soc. Jpn.* **2011**, *80*, SA110.
(53) Tokunaga, Y.; Homma, Y.; Kambe, S.; Aoki, D.; Sakai, H.; Yamamoto, E.; Nakamura, A.; Shiokawa, Y.; Walstedt, R. E.; Yasuoka, H. *Phys. Rev. Lett.* **2005**, *94*, 137209.
(54) Eastman, M. P.; Hecht, H. G.; Lewis, W. B. *J. Chem. Phys.* **1971**, *54*, 4141−4146.
(55) Yang, S.; Shore, J.; Oldfield, E. *J. Magn. Reson.* **1992**, *99*, 408−412.
(56) Golding, R. M.; Halton, M. P. *Aust. J. Chem.* **1972**, *25*, 2577−2581.
(57) Lewis, W. B.; Rabideau, S. W.; Krikorian, N. H.; Witteman, W. G. *Phys. Rev.* **1968**, *170*, 455−462.
(58) Magnani, N.; Santini, P.; Amoretti, G.; Caciuffo, R. *Phys. Rev. B* **2005**, *71*, 054405.
(59) Wybourne, B. G. *Spectroscopic Properties of Rare Earths;* Interscience: New York, 1965.
(60) Amoretti, G.; Blaise, A.; Caciuffo, R.; Fournier, J. M.; Hutchings, M. T.; Osborn, R.; Taylor, A. D. *Phys. Rev. B* **1989**, *40*, 1856.
(61) Amoretti, G.; Blaise, A.; Caciuffo, R.; Di Cola, D.; Fournier, J. M.; Hutchings, M. T.; Lander, G. H.; Osborn, R.; Severing, A.; Taylor, A. D. *J. Phys.: Condens. Matter* **1992**, *4*, 3459.
(62) Kern, S.; Robinson, R. A.; Nakotte, H.; Lander, G. H.; Cort, B.; Watson, P.; Vigil, F. A. *Phys. Rev. B* **1999**, *59*, 104.
(63) Karraker, D. G. *J. Chem. Phys.* **1975**, *63*, 3174−3175.
(64) Wadt, W. R. *J. Am. Chem. Soc.* **1981**, *103*, 6053−6057.
(65) Dyall, K. G. *Mol. Phys.* **1999**, *96*, 511−518.
(66) Infante, I.; Kovács, A.; La Macchia, G.; Rehaman Moughal Shahi, A.; Gibson, J. K.; Gagliard, L. *J. Phys. Chem. A* **2010**, *114*, 6007−6015.
(67) Teterin, A. Y.; Ryzhkov, M. V.; Teterin, Y. A.; Vukcevic, L.; Terekhov, V. A.; Maslakov, K. I.; Ivanov, K. E. *Nucl. Technol. Radiat. Prot.* **2008**, *2*, 34.
(68) Ward, A. L.; Buckley, H. L.; Lukens, W. W.; Arnold, J. *J. Am. Chem. Soc.* **2013**, *135*, 13965−13971.
(69) Adam, C.; Kaden, P.; Beele, B. B.; Müllich, U.; Trumm, S.; Geist, A.; Panak, P. J.; Denecke, M. A. *Dalton Trans.* **2013**, *42*, 14068−14074.